Porous and three-dimensional carbon aerogels from nanocellulose/pristine graphene for high-performance supercapacitor electrodes

Yaqi Wang
Wuhan University of Technology
Junwei Yang
Wuhan University of Technology
Yiheng Song
Wuhan University of Technology
Quanling Yang (yangql@whut.edu.cn)
Wuhan University of Technology
Chuanxi Xiong
Wuhan University of Technology
Zhuqun Shi
Wuhan University of Technology

Research Article

Keywords: nanocellulose, pristine graphene, carbon aerogel, electrical conductivity, supercapacitor

Posted Date: August 25th, 2022

DOI: https://doi.org/10.21203/rs.3.rs-1977044/v1

Abstract

Bio-based materials with good electrical properties produced by environmentally friendly methods have been increasingly applied in battery and supercapacitor technologies. In this work, we used 2,2,6,6-tetramethylpiperidine-1-oxyl (TEMPO)-oxidized cellulose nanofibers (TOCN) and pristine graphene (PG) as precursors to fabricate three-dimensional (3D) carbon aerogels with outstanding conductivity via freeze-drying followed by carbonization. The specific capacitance of the carbonized TOCN/PG (CTG) aerogels reached 134.09 F/g at a current density of 0.5 A/g. Meanwhile, a better cycling stability was achieved and the capacitance retained 98.89% after 5000 cycles. As the temperature increased to 1100°C, the electrochemical performance of the CTOCN-1100 electrode was improved significantly with a specific capacitance of 361.74 F/g at a current density of 0.5 A/g, and the capacitance still retained as high as 99.3% after 5000 cycles. Therefore, these bio-based cellulose nanofibrils are promising in the field of supercapacitors.

Introduction

In recent years, sustainable and environment-friendly concepts have received a lot of attention in the field of energy storage technologies. Renewable raw materials, green synthetic routes and environmentally friendly components are increasingly used in battery and supercapacitor technologies[Chio et al. 2014; Chung and Manthiram. 2014; Long et al. 2014]. As one of the most promising green nanomaterials[Siqueira et al. 2010; Qing et al. 2021; Ling et al. 2021; Chen et al. 2021], nanocellulose has great application value in different fields[Lao et al. 2018; Song et al. 2021; Yin et al. 2020; Zhang et al. 2014; Zheng et al. 2015; Liu et al. 2022; Song et al. 2022; Song et al. 2011; Xu et al. 2021] due to its outstanding mechanical strength, excellent flexibility and large aspect ratio[Chen et al. 2020; Isogai et al. 2011; Wu et al. 2012; Wu et al. 2021]. However, as an insulating material, the electrical conductivity of nanocellulose electrodes is difficult to meet the requirements of practical applications. Carbonization is an effective way to improve the electrical conductivity of biomass materials[Deng et al. 2013; Li et al. 2014; Wang et al. 2014; Gao et al. 2019; Song et al. 2019; Liu et al. 2020], and the high-temperature carbonization of nanocellulose under inert gas can effectively improve its electrical conductivity. However, the specific capacity of the neat carbonized nanocellulose is still limited when used as supercapacitor electrodes.

Improving the electrochemical properties of nanocellulose can be carried out from two aspects. On one hand, adding high surface area fillers to the nanocellulose matrix can effectively increase the specific surface area of nanocellulose-based composites, thus improving their electrochemical specific capacity[Yang et al. 2018; Jyothibasu et al. 2022; Liang et al. 2022]. As one of the most promising two-dimensional materials, graphene is widely used in the field of energy storage devices due to its excellent electrical conductivity, outstanding mechanical properties, high specific surface area and stable electrochemical properties[Ambrosi et al. 2014; Chen et al. 2013; Kanninen et al. 2016; Kim et al. 2011; Liu et al. 2013; Wang et al. 2014]. Previous experiments have shown that the nanocellulose (TOCN) prepared by 2,2,6,6-tetramethylpiperidine-1-oxyl (TEMPO)-oxidation method has a strong affinity for graphene as

well as dispersion effect due to the large number of surface functional groups (*e.g.* -COO^-) on its surface. It can effectively prevent the π-π stacking of graphene[Zhang et al. 2012], improve the electrolyte infiltration performance of graphene, and enhance the mesopore utilization of graphene materials[Jiang et al. 2017; Li et al. 2019; Li et al. 2021; Nie et al. 2018; Wu et al. 2012; Zhang et al. 2018]. On the other hand, three-dimensional carbon assemblies are considered as ideal supercapacitor electrode materials because of their good structural stability and rich internal pore structure. Using one-dimensional nanocellulose as the structural unit to construct nanocellulose aerogel with three-dimensional structure can greatly enhance the specific surface area and obtain rich porous microscopic morphology, which is also an effective way to endow nanocellulose with high electrochemical capacity.

In this work, TOCN/PG composite aerogels were prepared using pristine graphene (PG) exfoliated by the triethanolamine method[Chen et al. 2017] and TOCN as precursors. Then the aerogels were carbonized at 750°C and 1100°C under argon atmosphere to obtain carbonized TOCN/PG composite aerogels. The effects of different PG contents and carbonization temperatures on the structures and properties of the carbonized aerogels were investigated by recent testing techniques. The electrochemical properties of the carbonized TOCN/PG composite aerogels were tested as working electrodes for supercapacitors, and the value of the method for realizing the production of nanocellulose-based high-performance supercapacitors was explored.

Experimental

Materials

A softwood-bleached kraft pulp (SBKP) was obtained from Nippon Paper Industries (Tokyo, Japan) with a water content of 80%. TEMPO (98%) was purchased from Sigma-Aldrich (St. Louis, USA). Sodium bromide (NaBr, AR), sodium hydroxide (NaOH, AR), sodium nitrate ($NaNO_3$, AR), hydrochloric acid (HCl, AR), anhydrous ethanol (AR), and tert-butanol (AR) were purchased from Sinopharm Chemical Reagent Co., Ltd. (China). Sodium hypochlorite (NaClO, AR), triethanolamine (AR, 98%), N, N-dimethylformamide (DMF, purity > 99.9%) were purchased from Aladdin (Shanghai, China). Graphite powder (325 mesh, 98%) was purchased from Nanjing Xianfeng Nano Technology Co., LTD. Nafion (5% W/W) was purchased from Kunshan Yisheng International Trade Co., LTD. Alumina powder (50 nm) and polished flannelette were bought from Shanghai Chenhua Instrument Co., LTD.

Preparation of TOCN dispersions

TEMPO-oxidized cellulose (TOC) from SBKP was prepared using the TEMPO/NaBr/NaClO system[Isogai. 2021]. 4.34 g TOC with 81% water content was added to 150 mL deionized water, stirred magnetically for 30 min and then sonicated for 6 min to achieve a uniform TOCN dispersion in the deionized water. Finally, the undispersed TOCN was removed by centrifugation to obtain a stable dispersion of 0.5 wt.% TOCN.

Preparation of PG

0.6 g of flake graphite powder and 60 mL of triethanolamine were added in a 100 mL single-necked flask and mechanically stirred at 1000 rpm for 8 h. Then the dispersion was centrifuged at 4500 rpm for 30 min to obtain the supernatant. The supernatant was mixed with deionized water and filtered under vacuum on a 0.22 μm pore size mixed cellulose ester membrane and washed three times with deionized water. The final filtrate was then dispersed in deionized water and freeze-dried to obtain the black PG powder.

Preparation of TOCN/PG aerogels

The PG powder was weighed in 100 g of 0.5% TOCN dispersion according to the mass fraction of PG (PG content in solid) of 5%, 10%, 15% and 20%, respectively. The mixture was stirred magnetically for 1 h and then sonicated for 4 min to disperse uniformly. The dispersion was poured into the mold and placed in HCl atmosphere for a period of time to obtain the nanocellulose-based hydrogel. It was then replaced with ethanol and tert-butanol in turn, and finally the TOCN/PG aerogel was obtained after freeze-drying for 48 h.

Preparation of carbonized TOCN/PG aerogels

TOCN/PG aerogels of different components were placed in a tubular furnace and heated to 750 ℃ for 2 h under argon atmosphere to obtain the carbonized TOCN/PG aerogels, denoted as CTG-750. Carbonized aerogels with PG content of 0%, 5%, 10%, 15% and 20% were denoted as CTOCN-750, CTG5-750, CTG10-750, CTG15-750 and CTG20-750, respectively. Then, TOCN aerogel and TOCN/PG aerogel with the best composition were carbonized at 1100 ℃ in the same condition, and the obtained carbonized aerogel were denoted as CTOCN-1100 and CTG-1100 respectively.

Preparation of working electrodes for supercapacitors

The surface of the glassy carbon electrode was polished with 50 nm diameter alumina powder before the experiment, and washed with ethanol. Then, 5 mg of the above carbonized aerogel was dispersed in 1 mL of DMF, and 5 μL of Nafion solution was added dropwise to increase the adhesion of the material. 1.5 μL of the above dispersion was applied to the electrode area on the surface of the glassy carbon electrode after stirring well, and when the solvent was dried, the electrode was ready for electrochemical testing.

Characterization

A Hitachi S-4800 field emission scanning electron microscope (Japan) was used to observe the internal microscopic morphology of the samples. Raman spectroscopy was performed using a Renishaw Raman microscope (UK) with a laser source wavelength of 514.5 nm. The specific surface area and pore distribution of the aerogel were tested by the ASAP 2020M specific surface area and pore analyzer (Micromeritics, USA). A three-electrode system was composed of Ag/AgCl as reference electrode, platinum wire as counter electrode, carbonized aerogel material as working electrode, and 1 mol/L H_2SO_4 aqueous solution as electrolyte. The electrode material was tested by CHI 660E electrochemical workstation (Shanghai Chenhua) for cyclic voltammetry, galvanostatic charge–discharge cycling, and impedance analysis.

Results And Discussion

Structural analysis of carbonized TOCN/PG aerogels

SEM images of different carbonized aerogels are shown in Fig. 1. General carbonization usually leads to the collapse of internal network structure of aerogels[Wang et al. 2022]. However, the uniform and obvious network pore structure was observed from Fig. 1a, which indicated that TOCN aerogel can still maintain its rich pore structure after carbonization at 750 ℃. This may be because the aerogel prepared by freeze-drying can avoid the shortcomings of direct heat treatment and retain open porous network. When the carbonization temperature was increased to 1100 ℃, the pores of the aerogel became smaller and more abundant (Fig. 1b). Figure 1c showed that after the compounding of TOCN and 10% PG, PG didn't destroy the TOCN pores and still maintained a good three-dimensional network structure, while the presence of TOCN blocked the self-stacking of PG to a certain extent. However, after carbonized at 1100 ℃, the three-dimensional structure was almost invisible in Fig. 1d, showing more of a stacked graphite structure in sheets. This phenomenon may be due to the further disappearance of the characteristic functional groups on the molecular surface of the TOCN between the PG sheets after carbonized at higher temperatures. The spatial resistance between the graphene nanosheets decreased, and the PG stacking occurred due to the strong van der Waals forces between the nanosheets. This destroyed the three-dimensional network structure of the aerogel. When the content of PG increased to 20%, the distance between graphene nanosheets was further reduced, and the nanosheets were agglomerated due to the excess, destroying the pore structure of the aerogel (Fig. S1).

To investigate the internal carbon atom structure of different aerogels at different carbonization temperatures, Raman spectroscopy tests were performed on CTOCN-750, CTOCN-1100, CTG10-750 and CTG10-1100, and the results were shown in Fig. 2. Normally, the D peak in the Raman diagram indicates the disorder and the degree of defects of carbon atoms, and the G peak indicates the sp^2 hybridized structure of carbon atoms, which is caused by the symmetry and crystallinity of carbon materials. The I_D/I_G is generally used to indicate the degree of defects in the material. The calculated I_D/I_G values were shown in Table S1. The results indicated that the values of I_D/I_G of TOCN increased significantly after increasing the carbonization temperature, which was due to that the higher carbonization temperature made the carbonization more complete and the characteristic functional groups on the surface further disappeared, thus increasing the surface defects. But the increasing of surface defects may exist in the form of pores and increase the specific surface area of the material. After adding PG to TOCN, the I_D/I_G value decreased due to the perfect crystal structure of PG nanosheets which increased the material orderliness. For the CTG10 aerogel, the carbonized nanocellulose sandwiched between PG nanosheets played the role of hindering graphene stacking, and the increase of carbonization temperature further reduced its surface characteristic functional groups, thus decreasing the hindrance between graphene sheets, leading to the stacking and agglomeration of graphene due to strong π-π interactions between the sheets. The appearance of a large number of relatively regular graphite-like structures inside the material

destroyed the internal three-dimensional structure. The I_D/I_G of CTG10-1100 (*i.e.*, 0.77) was therefore much lower than that of CTG10-750 (*i.e.*, 1.14).

To further investigate the internal microstructure of the composite aerogels, nitrogen adsorption/desorption isotherm tests were performed on CTOCN-750, CTG10-750, CTG10-1100, CTG20-750 and CTOCN-1100, respectively (Fig. 3). And the specific surface area and pore volume of the carbonized aerogels were shown in Table S2. The specific surface area of CTOCN-750 aerogel were 457.9 m^2/g and pore volume were 0.79 cm^3/g, exhibiting a more abundant pore structure. With the increase of PG content, the specific surface area and pore volume of aerogel gradually decreased, and at the PG content of 20 wt%, the specific surface area and pore volume of CTG20-750 aerogel decreased to 192.4 m^2/g and 0.28 cm^3/g, respectively, and the three-dimensional structure was substantially destroyed. After increasing the carbonization temperature to 1100°C, the specific surface area and pore volume of CTG10-1100 were further reduced due to the further disappearance of oxygen-containing functional groups on the surface of TOCN and the reduction of PG layer-to-layer resistance, which made the self-stacking effect of graphene more obvious and disrupted the internal network structure of the material. In general, increasing the PG content and raising the carbonization temperature both decreased the aerogel specific surface area and pore volume. The specific surface area and pore volume of CTG10-750 were reduced but can still maintain a certain three-dimensional network structure, while CTG10-1100 and CTG20-750 aerogels decreased significantly, and the three-dimensional network structure was destroyed, which was consistent with the SEM results.

Electrochemical properties of carbonized TOCN/PG aerogels

Cyclic voltammetry (CV) was performed by applying an external voltage to the electrode material for cyclic scanning to obtain response current versus scanning voltage curves, thus visualizing the voltage window, reversibility and capacitive behavior of the supercapacitor response. Figure 4 showed the CV curves of the carbonized aerogels at different scan rates. It can be observed that the CV curves of the four components of CTG-750 aerogel were all symmetrical rectangular shapes, reflecting a relatively ideal double electric layer capacitance behavior. Meanwhile, there was a small symmetrical redox peak on the curves, which maybe because the carbonization treatment didn't completely remove the oxygen-containing functional groups on the surface of cellulose. Thus, the electrode material exhibited a certain pseudo capacitance effect. At different scanning rates, CV curves all presented good rectangles and symmetries. With the increase of scanning rates, the contour of curves almost didn't change, and the corresponding current increased linearly. Even at the scanning rate of 100 MV/s, CV curves still showed rectangle-like shapes. This indicated that the internal structure of CTG-750 electrode material had little resistance to charge transfer and electrolyte ion diffusion, and can work with large current. The strong π-π interaction between PG molecules made it easy to agglomerate. Although increasing the amount of PG can improve the overall electrical conductivity of the material, it also destroyed the pore structure of the material to a certain extent, thus increasing the electron and ion transport resistance. Therefore, when the

PG content reached 20%, the CV curve of the material appeared obvious distortion, and the response current decreased greatly.

When the carbonization temperature increased to 1100°C, the CV curve of CTOCN-1100 exhibited an almost perfect rectangular curve (Fig. 4e) and the redox peak on the surface almost disappeared, indicating that with the increase of the carbonization temperature, the characteristic functional groups on the surface of cellulose were carbonized more completely and closer to a double-layer capacitor. However, due to the further reduction of oxygen-containing functional groups on the cellulose surface, the resistance between PG layers decreased, which made the self-stacking effect of graphene more obvious. This destroyed the internal network structure of CTG10-1100 and increased the internal resistance, thus affecting the electrochemical performance of the electrode material and obtaining a twisted CV curve (Fig. 4f).

The galvanostatic charge-discharge curves of the carbonized aerogels at different current densities were shown in Fig. 5. The mass capacitance under different current densities was calculated according to the charge-discharge curves (Fig. 6). It can be observed from the figures that the galvanostatic charge-discharge curves of all aerogel components under different current densities were relatively symmetric triangles, showing an ideal capacitance behavior. But at each moment of charge-discharge conversion, there was a small voltage drop, which was determined by the material and the internal resistance of the capacitor itself. The addition of PG can effectively reduce the resistance of the material. So with the increase of PG, the voltage drop gradually decreased. When the content of PG was over 10%, PG agglomerated due to the excess, which destroyed the internal network structure of the material and increased the ion transport resistance, making the voltage drop larger. At the current density of 0.5 A/g, the specific capacity of CTG10-750 reached 134.09 F/g, which was much higher than that of CTOCN-750 (92.65 F/g) and CTG20-750 (50.08 F/g) (Fig. 6a). In addition, with the increase of current density, the specific capacity of all materials would be attenuated due to the internal resistance of the whole capacitor system. When the current density increased, the response speed was slow, which affected the expression of capacity. In this work, when the current density was increased to 10 A/g, CTG10-750 still had a specific capacity of 96.3F /g and a capacity retention rate of 71.82%, which was higher than those of other components.

Compared with the properties of electrode materials carbonized at 750 ℃, the voltage drop of carbonized TOCN aerogel at 1100 ℃ was small, and the specific capacity increased significantly, reaching 361.74 F/g at 0.5 A/g (Fig. 6b). While the constant current charge-discharge curve of CTG10-1100 showed a significant voltage drop, and the specific capacitance value reduced by about 6 times. The above phenomenon was mainly because when TOCN was carbonized at higher temperature, the remaining uncarbonized oxygen-containing functional groups were further reduced and the electrical conductivity was increased. Meanwhile, the disappearance of oxygen-containing functional groups formed pores inside the material, providing more paths for ion transport, reducing the internal resistance and increasing the charge and ion transport efficiency. However, the conductivity of PG in CTG10-1100 didn’t increase significantly due to the decrease of oxygen-containing functional groups inside. Combined with SEM

results (Fig. 1d), PG aggregated observably due to the decrease of functional groups on cellulose surface, which destroyed the three-dimensional network structure inside the aerogel and increased the charge transfer resistance.

Electrochemical impedance spectroscopy (EIS) is an important way to study the electrochemical performance of supercapacitors. Figure 7a showed Nyquist impedance diagrams of different components CTG-750 aerogel measured at open circuit voltage in the frequency range of 0.01-100000 Hz. It can be observed from Nyquist impedance spectrum that, in the high frequency region, the intersection of the Nyquist impedance spectra with the X-axis for all materials was near 4 Ω, indicating that adding appropriate adhesive to electrode material can effectively reduce the interface contact resistance. In the intermediate frequency region, CTG10-750 exhibited a relatively small Warburg impedance, which was due to the fact that for carbonized TOCN aerogels, the addition of PG can effectively improve the electrical conductivity of the material and strengthen the charge transfer efficiency on the material surface. But PG itself was easy to stack and had limited compatibility with TOCN. With the further increase of PG addition, aggregation occurred due to the excess, which destroyed the three-dimensional network structure inside the material and affected electron ion transport.

The Warburg impedance of CTOCN-1100 aerogel in the intermediate frequency region decreased a lot compared with that of CTOCN-750 when the carbonization temperature was increased to 1100°C. This is because increasing the carbonization temperature can further remove the characteristic functional groups on the surface of TOCN. On one hand, it can effectively improve the conductivity of the carbonized cellulose aerogel and enhance the charge transmission efficiency on the material surface. On the other hand, it can also enrich the pore structure inside the material, which can provide more channels for the diffusion of electrolyte ions in the electrode material, and improve the ion diffusion efficiency. The internal resistance of CTOCN-1100 aerogel material can be greatly reduced through the synergistic action. However, for CTG10-1100 aerogel, the specific surface area and pore volume of the material were significantly reduced by increasing the carbonization temperature. The agglomeration effect of PG nanosheets destroyed the three-dimensional pore structure inside the material, hindered ion diffusion and increased the internal resistance. Therefore, CTG10-1100 had a large Warburg impedance.

The cycling stability results are shown in Fig. 8. The specific capacitance of CTOCN-750 and CTG10-750 remained at the initial 98.20% and 98.89%, respectively, after 5000 cycles (Fig. 8a), indicating a good cycling stability. Combined with the SEM morphology analysis, the better cycling stability of CTOCN-750 and CTG10-750 aerogels were mainly based on the continuous porous three-dimensional network structure inside the aerogels. Figure 8b showed that the specific capacitance retention of CTOCN-1100 electrode material reached 99.30% after 5000 cycles, which was higher than CTOCN-750 due to its higher conductivity and richer internal interlaced pore structure. However, the capacitance retention of CTG10-1100 carbonized at 1100 ℃ was reduced to 82.00%. Combined with the SEM morphology analysis, it suggested that this phenomenon was due to the further disappearance of characteristic functional groups on the cellulose surface, which made the PG nanosheets agglomerate. This destroyed the three-

dimensional network structure of the aerogels, increased the internal resistance and hindered ion transport.

Conclusion

In this work, TOCN/PG carbon aerogels were obtained by gel formation, freeze-drying, and then carbonization at high temperature. With the increase of PG content, the electrochemical performance of the aerogel electrode material improved significantly. The specific capacitance of CTG10-750 reached 134.09 F/g at a current density of 0.5 A/g. Meanwhile, a better cycling stability was achieved and the capacitance retained 98.89% after 5000 cycles. As the temperature increased to 1100°C, the electrochemical performance of the CTOCN-1100 electrode was improved observably with a specific capacitance of 361.74 F/g at a current density of 0.5 A/g and the capacitance retained as high as 99.3% after 5000 cycles. Owing to the outstanding electrochemical performance, low cost and eco-friendliness, the CTOCN aerogels are believed to be a promising electrode material for supercapacitors.

Declarations

Consent for publication

Not applicable.

Availability of data and materials

All data generated or analysed during this study are included in this published article and its supplementary information files.

Funding

The research was supported by the Hainan Provincial Joint Project of Sanya Yazhou Bay Science and Technology City (Grant No: 520LH017), Sanya Science and Education Innovation Park of Wuhan University of Technology (2021KF0015), and State Key Laboratory for Modification of Chemical Fibers and Polymer Materials (KF2213).

Competing Interest

The authors report no declarations of interest.

Acknowledgments

The research was supported by the Hainan Provincial Joint Project of Sanya Yazhou Bay Science and Technology City (Grant No: 520LH017), Sanya Science and Education Innovation Park of Wuhan University of Technology (2021KF0015), and State Key Laboratory for Modification of Chemical Fibers and Polymer Materials (KF2213).

Author Contributions

Yaqi Wang: Methodology, Validation, Formal analysis, Writing - original draft, Investigation. **Junwei Yang**: Validation, Investigation. **Yiheng Song**: Writing - Review & Editing. **Quanling Yang**: Conceptualization, Methodology, Writing - Review & Editing, Project administration, Supervision. **Chuanxi Xiong**: Writing - Review & Editing. **Zhuqun Shi**: Writing - Review & Editing.

Compliance with ethical standards

Conflict of interest: The authors declare that they have no conflict of interest.

Ethical approval: The study was approved by the Ethics Committee of Wuhan University of Technology. The article does not contain any experiments with human participants or animals performed by any of the authors.

Informed consent: Informed consent was obtained from all individual participants included in the study.

References

1. Ambrosi A, Chua CK, Bonanni A, Pumera M (2014) Electrochemistry of graphene and related materials. Chem. Rev 114(14): 7150-7188. https://doi.org/10.1021/cr500023c
2. Chen H, Liu B, Yang Q, Wang S, Liu W, Zheng X, Liu Z, Liu L, Xiong C (2017) Facile one-step exfoliation of large-size 2D materials via simply shearing in triethanolamine. Mater. Lett. 199(15): 124-127. https://doi.org/10.1016/j.matlet.2017.04.066
3. Chen J, Li C, Shi G (2013) Graphene materials for electrochemical capacitors. J. Phys. Chem. Lett. 4(8): 1244-1253. https://doi.org/10.1021/jz400160k
4. Chen J, Liu Y, Liu Z, Chen Y, Zhang C, Yin Y, Yang Q, Shi Z, Xiong C (2020) Carbon nanofibril composites with high sulfur loading fabricated from nanocellulose for high-performance lithium-sulfur batteries. Colloids Surf. A Physicochem. Eng. Asp. 603(20): 125249. https://doi.org/10.1016/j.colsurfa.2020.125249
5. Chen L, Cao S, Huang L, Wu H, Hu H, Liu K, Lin S (2021) Development of bamboo cellulose preparation and its functionalization. Journal of Forestry Engineering 6(4): 1-13. https://doi.org/10.13360/j.issn.2096-1359.202104011
6. Chung SH, Manthiram A (2014) Carbonized eggshell membrane as a natural polysulfide reservoir for highly reversible Li-S batteries. Adv. Mater. 26(9): 1360-1365. https://doi.org/10.1002/adma.201304365
7. Choi KH, Cho SJ, Chun SJ, Yoo JT et al (2014) Heterolayered, one-dimensional nanobuilding block mat batteries. Nano Lett. 14(10): 5677-5686. https://doi.org/10.1021/nl5024029
8. Deng L, Young RJ, Kinloch IA, Zhu Y, Eichhorn SJ (2013) Carbon nanofibres produced from electrospun cellulose nanofibers. Carbon 58: 66-75. https://doi.org/10.1016/j.carbon.2013.02.032

9. Gao K, Zhao S, Niu Q, Wang L (2019) 2D nitrogen-doped porous carbon nanosheets derived from cellulose nanofiber/silk fibroin nanohybrid cellular monoliths with promising capacitive performance. Cellulose 26: 9241–9254. https://doi.org/10.1007/s10570-019-02723-3
10. Isogai A (2021) Emerging nanocellulose technologies: recent developments. Adv. Mater. 33(28): 2000630. https://doi.org/10.1002/adma.202000630
11. Isogai A, Saito T, Fukuzumi H (2011) TEMPO-oxidized cellulose nanofibers. Nanoscale 3: 71-85. https://doi.org/10.1039/c0nr00583e
12. Jiang Q, Kacica C, Soundappan T, Liu KK, Tadepalli S, Biswas P, Singamaneni S (2017) An in situ grown bacterial nanocellulose/graphene oxide composite for flexible supercapacitors. J. Mater. Chem. A 5(27): 13976-13982. https://doi.org/10.1039/c7ta03824k
13. Jyothibasu JP, Wang RH, Ong K et al (2022) Scalable synthesis of γ-Fe_2O_3–based composite films as freestanding negative electrodes with ultra-high areal capacitances for high-performance asymmetric supercapacitors. Cellulose 29: 321–340. https://doi.org/10.1007/s10570-021-04298-4
14. Kanninen P, Luong ND, Sinh LH, Anoshkin IV, Tsapenko A, Seppala J, Nasibulin AG, Kallio T (2016) Transparent and flexible high-performance supercapacitors based on single-walled carbon nanotube films. Nanotechnology 27: 235403. https://doi.org/10.1088/0957-4484/27/23/235403
15. Kim TY, Lee HW, Stoller M, Dreyer DR, Bielawski CW, Ruoff RS, Suh KS (2011) High-performance supercapacitors based on poly(ionic liquid)-modified graphene electrodes. ACS Nano 5(1): 436-442. https://doi.org/10.1021/nn101968p
16. Lao J, Xie H, Shi Z, Li G, Li B, Hu G-H, Yang Q, Xiong C (2018) Flexible regenerated cellulose/boron nitride nanosheet high-temperature dielectric nanocomposite films with high energy density and breakdown strength. ACS Sustainable Chem. Eng. 6(5): 7151-7158. https://doi.org/10.1021/acssuschemeng.8b01219
17. Li M, Miao Y, Zhai X, Yin Y, Zhang Y, Jian Z, Wang X, Sun L, Liu Z (2019) Preparation of and research on bioinspired graphene oxide/nanocellulose/polydopamine ternary artificial nacre. Mater. Des. 181(5): 107961. https://doi.org/10.1016/j.matdes.2019.107961
18. Li M, Wang X, Zhao R, Miao Y, Liu Z (2021) A novel graphene-based micro/nano architecture with high strength and conductivity inspired by multiple creatures. Sci. Rep. 11: 1-15. https://doi.org/10.1038/s41598-021-80972-8
19. Li Y, Zhu H, Shen F, Wan J, Han X, Dai J, Dai H, Hu L (2014) Highly conductive microfiber of graphene oxide templated carbonization of nanofibrillated cellulose. Adv. Funct. Mater. 24(46): 7366-7372 https://doi.org/10.1002/adfm.201402129.
20. Liang C, Zang L, Shi F et al (2022) High-performance cotton fabric-based supercapacitors consisting of polypyrrole/Ag/graphene oxide nanocomposite prepared via UV-induced polymerization. Cellulose 29: 2525–2537. https://doi.org/10.1007/s10570-022-04454-4
21. Ling Z, Lai C, Huang C, Xu F, Yong Q (2021) Research progress in variations of cellulose supramolecular structures via biomass pretreatment. Journal of Forestry Engineering 6(4): 24-34. https://doi.org/10.13360/j.issn.2096-1359.202006024

22. Liu D, Gao Y, Song Y, Zhu H, Zhang L, Xie Y, Shi H, Shi Z, Yang Q, Xiong C (2022) Highly sensitive multifunctional electronic skin based on nanocellulose/MXene composite films with good electromagnetic shielding biocompatible antibacterial properties. Biomacromolecules 23(1): 182-195. https://doi.org/10.1021/acs.biomac.1c01203
23. Liu H, Huang J, Li X, Liu J, Zhang Y (2013) Graphene as a high-capacity anode material for lithium ion batteries. Journal of Wuhan University of Technology-Materials Science Edition 28: 220-223. https://doi.org/10.1007/s11595-013-0668-7
24. Liu L, Hu S, Gao K (2020) Natural nanofiber-based stacked porous nitrogen-doped carbon/$NiFe_2O_4$ nanohybrid nanosheets. Cellulose 27: 1021–1031. https://doi.org/10.1007/s10570-019-02843-w
25. Long C, Chen X, Jiang L, Zhi L, Fan Z (2015) Porous layer-stacking carbon derived from in-built template in biomass for high volumetric performance supercapacitors. Nano Energy 12: 141-151. https://doi.org/10.1016/j.nanoen.2014.12.014
26. Nie S, Zhang K, Lin X, Zhang C, Yan D, Liang H, Wang S (2018) Enzymatic pretreatment for the improvement of dispersion and film properties of cellulose nanofibrils. Carbohydr. Polym. 181: 1136-1142. https://doi.org/10.1016/j.carbpol.2017.11.020
27. Qing Y, Liao Y, Liu J, Tian C, Xu H, Wu Y (2021) Research progress of wood-derived energy storage materials. Journal of Forestry Engineering 6(5): 1-13. https://doi.org/10.13360/j.issn.2096-1359.202012046
28. Siqueira G, Bras J, Dufresne A (2010) Cellulosic bionanocomposites: A review of preparation, properties and applications. Polymers-Basel 2(4): 728-765. https://doi.org/10.3390/polym2040728
29. Song P, Shen X, He X et al (2019) Cellulose-derived nitrogen-doped hierarchically porous carbon for high-performance supercapacitors. Cellulose 26: 1195–1208. https://doi.org/10.1007/s10570-018-2115-6
30. Song Y, Bao J, Hu Y, Cai H, Xiong C, Yang Q, Tian H, Shi Z (2022) Forward polarization enhanced all-polymer based sustainable triboelectric nanogenerator from oriented electrospinning PVDF/cellulose nanofibers for energy harvesting. Sustain. Energy Fuels 6(9): 2377-2386. https://doi.org/10.1039/D2SE00321J
31. Song Y, Shi Z, Hu G-H, Xiong C, Isogai A, Yang Q (2021) Recent advances in cellulose-based piezoelectric and triboelectric nanogenerators for energy harvesting: A review. J. Mater. Chem. A 9(4): 1910-1937. https://doi.org/10.1039/d0ta08642h
32. Song Y, Wu T, Bao J, Xu M, Yang Q, Zhu L, Shi Z, Hu G-H, Xiong C (2022) Porous cellulose composite aerogel films with super piezoelectric properties for energy harvesting. Carbohydr. Polym. 288: 119407. https://doi.org/10.1016/j.carbpol.2022.119407
33. Wang K, Li L, Zhang T, Liu Z (2014) Nitrogen-doped graphene for supercapacitor with long-term electrochemical stability. Energy 70: 612-617. https://doi.org/10.1016/j.energy.2014.04.034
34. Wang L, Wu Q, Zhao B, Li Z, Zhang Y, Huang L, Yu S (2022) Multi-functionalized carbon aerogels derived from chitosan. J. Colloid Interface Sci. 605: 790-802. https://doi.org/10.1016/j.jcis.2021.07.132

35. Wang LP, Schutz C, Salazar-Alvarez G, Titirici MM (2014) Carbon aerogels from bacterial nanocellulose as anodes for lithium ion batteries. RSC Adv. 4(34): 17549-17554. https://doi.org/10.1039/c3ra47853j
36. Wu CN, Saito T, Fujisawa S, Fukuzumi H, Isogai A (2012) Ultrastrong and High Gas-Barrier Nanocellulose/Clay-Layered Composites. Biomacromolecules 13(6): 1927-1932. https://doi.org/10.1021/bm300465d
37. Wu T, Song Y, Shi Z, Liu D, Chen S, Xiong C, Yang Q (2021) High-performance nanogenerators based on flexible cellulose nanofibril/MoS_2 nanosheet composite piezoelectric films for energy harvesting. Nano Energy 80: 105541. https://doi.org/10.1016/j.nanoen.2020.105541
38. Wu ZS, Yang S, Sun Y, Parvez K, Feng X, Mullen K (2012) 3D nitrogen-doped graphene aerogel-supported Fe_3O_4 nanoparticles as efficient eletrocatalysts for the oxygen reduction reaction. J. Am. Chem. Soc. 134(22): 9082-9085. https://doi.org/10.1021/ja3030565
39. Xu M, Wu T, Song Y, Jiang M, Shi Z, Xiong C, Yang Q (2021) Achieving high-performance energy harvesting and self-powered sensing in flexible cellulose nanofibril/MoS_2/$BaTiO_3$ composite piezoelectric nanogenerators. J. Mater. Chem. C 9(43): 15552-15565. https://doi.org/10.1039/D1TC03886A
40. Yang J, Xie H, Chen H, Shi Z, Wu T, Yang Q, Xiong C (2018) Cellulose nanofibril/boron nitride nanosheet composites with enhanced energy density and thermal stability by interfibrillar cross-linking through Ca^{2+}. J. Mater. Chem. A 6(4): 1403–1411. https://doi.org/10.1039/c7ta08188j
41. Yin Y, Zhang C, Yu W, Kang G, Yang Q, Shi Z, Xiong C (2020) Transparent and flexible cellulose dielectric films with high breakdown strength and energy density. Energy Stor. Mater. 26: 105-111. https://doi.org/10.1016/j.ensm.2019.12.034
42. Zhang K, Zhang Y, Yan D, Zhang C, Nie S (2018) Enzyme-assisted mechanical production of cellulose nanofibrils: thermal stability. Cellulose 25: 5049-5061. https://doi.org/10.1007/s10570-018-1928-7
43. Zhang L, Zhao X, Stoller MD, Zhu Y, Ji H, Murali S, Wu Y, Perales S, Clevenger B, Ruoff RS (2012) Highly conductive and porous activated reduced graphene oxide films for high-power supercapacitors. Nano Lett. 12(4): 1806-1812. https://doi.org/10.1021/nl203903z
44. Zhang X, Lin Z, Chen B, Zhang W, Sharma S, Gu W, Deng Y (2014) Solid-state flexible polyaniline/silver cellulose nanofibrils aerogel supercapacitors. J. Power Sources 246: 283-289. https://doi.org/10.1016/j.jpowsour.2013.07.080
45. Zheng Q, Cai Z, Ma Z, Gong S (2015) Cellulose nanofibril/reduced graphene oxide/carbon nanotube hybrid aerogels for highly flexible and all-solid-state supercapacitors. ACS Appl. Mater. Interfaces 7(5): 3263-3271. https://doi.org/10.1021/am507999s

Figures

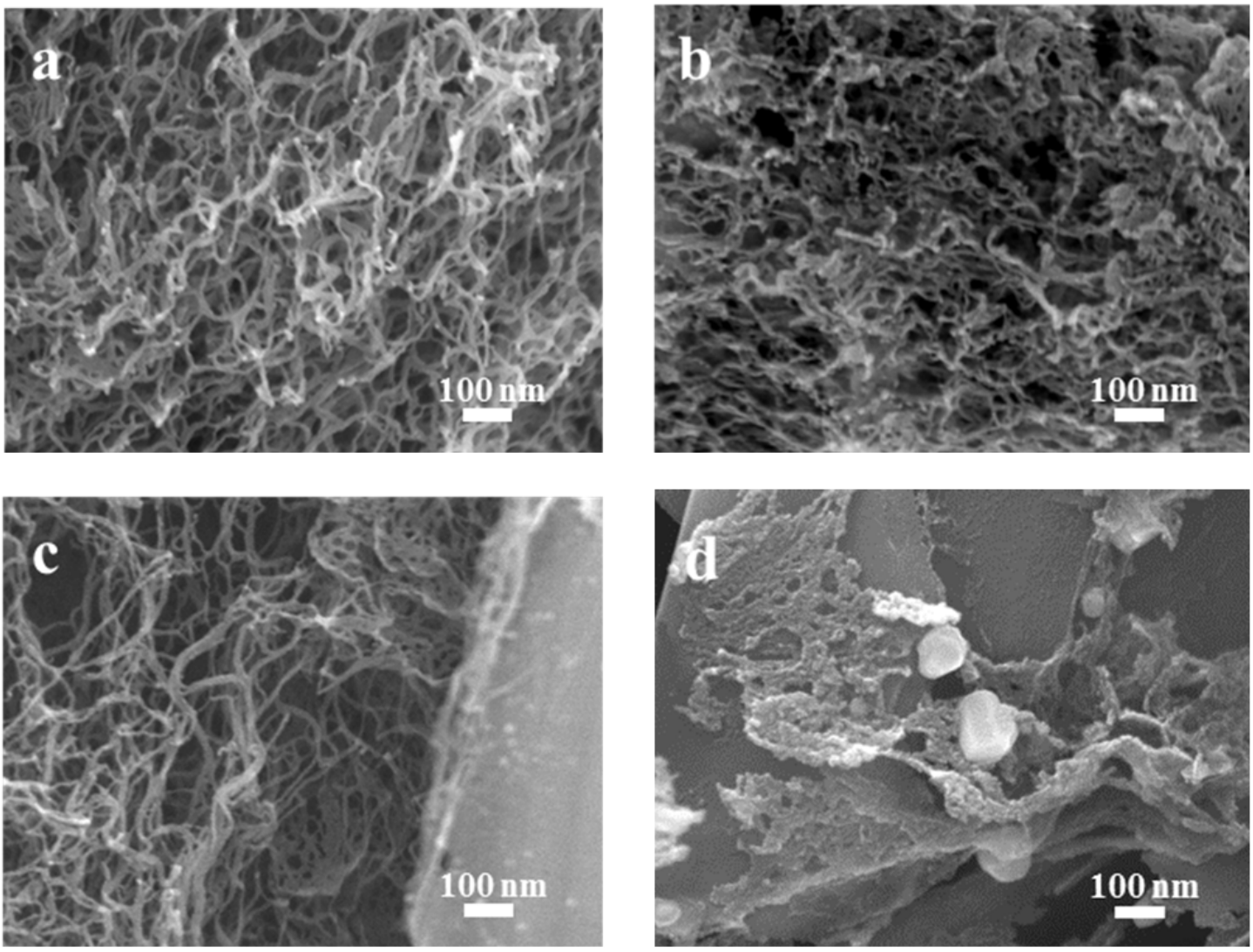

Figure 1

SEM images (×100 k) of (a) CTOCN-750, (b) CTOCN-1100, (c) CTG10-750, (d) CTG10-1100

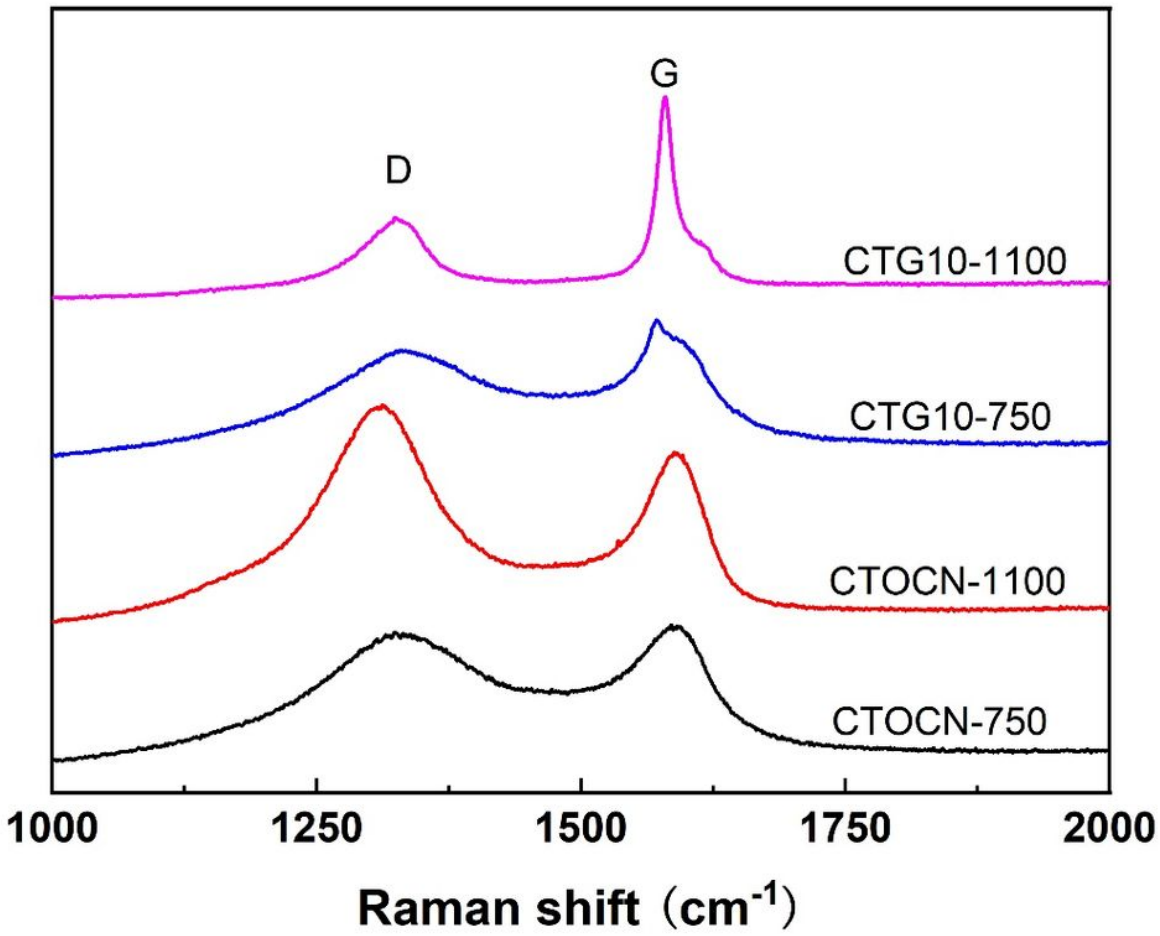

Figure 2

Raman spectra of carbonized TOCN and TOCN/PG aerogels

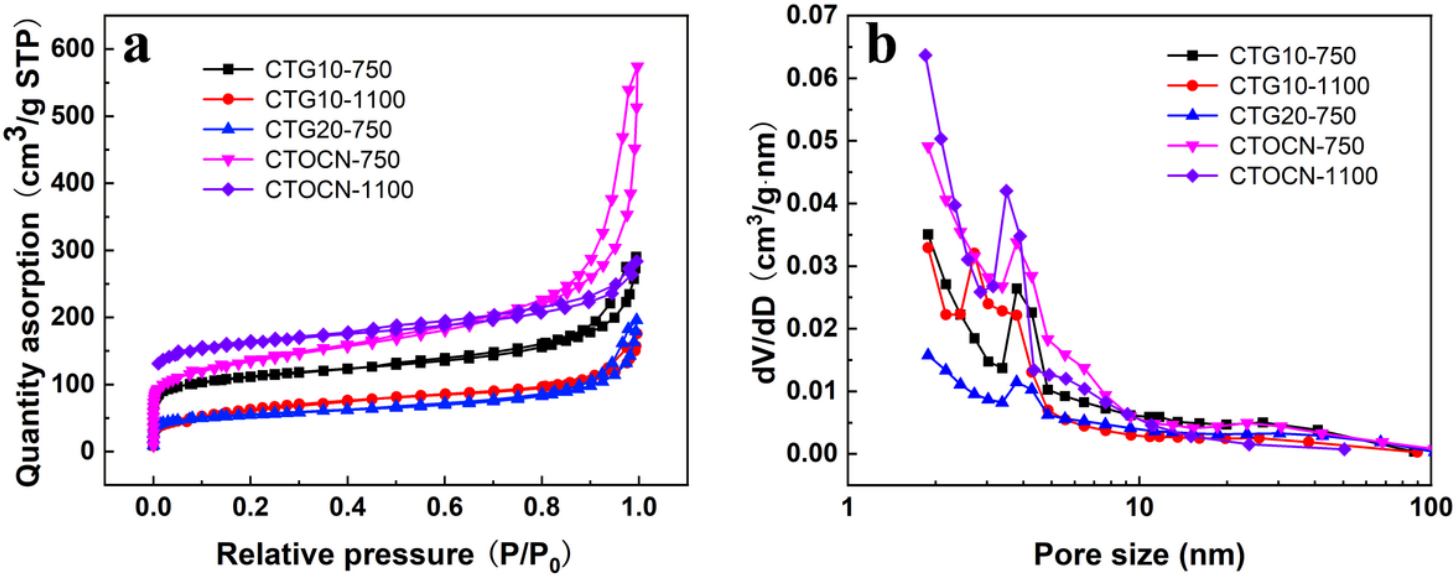

Figure 3

(a) Nitrogen adsorption/desorption isotherms and (b) Barrett-Joyner-Halenda (BJH) pore size distribution of CTOCN-750, CTG10-750, CTG10-1100, CTG20-750 and CTOCN-1100 aerogels

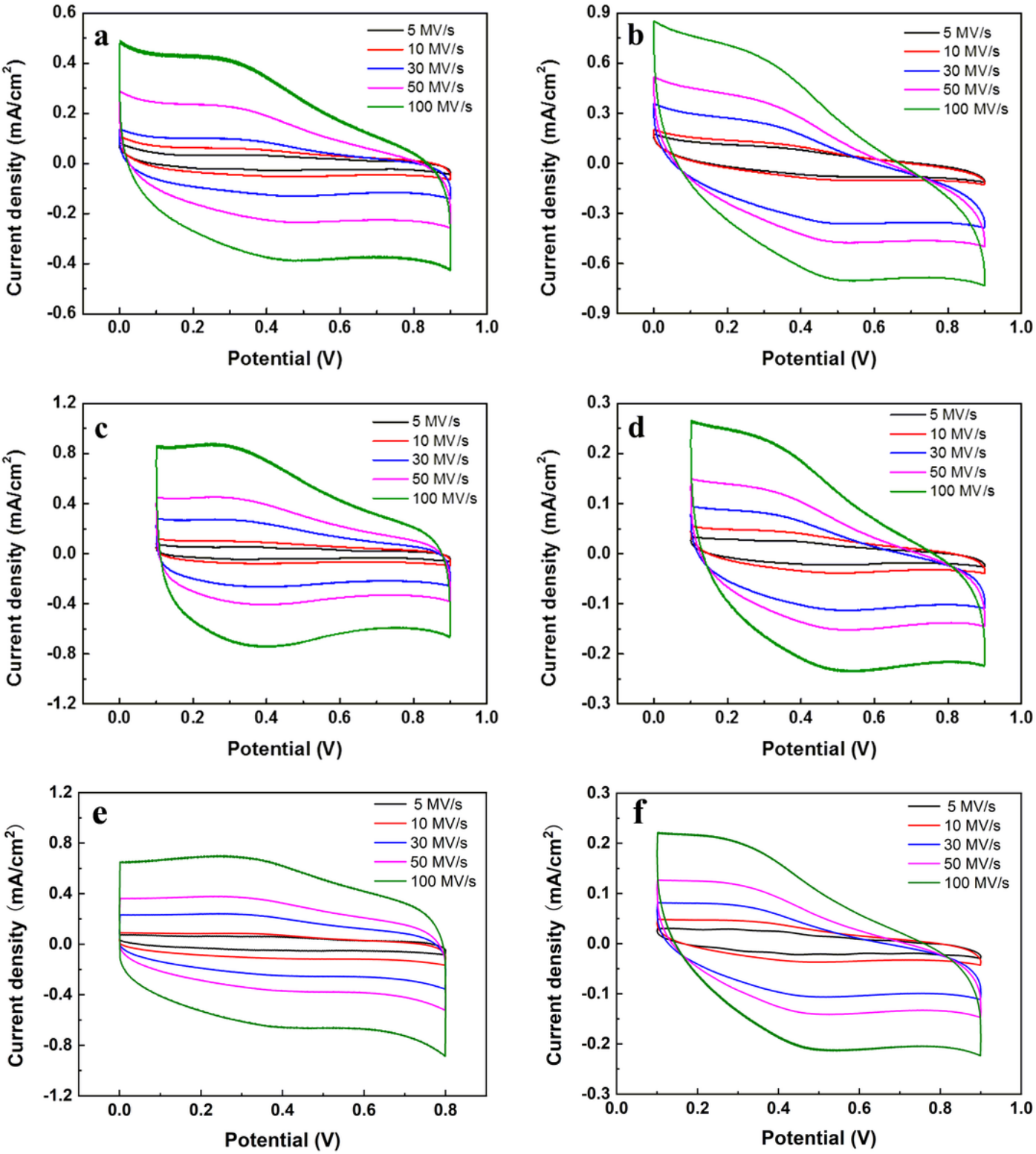

Figure 4

Cyclic voltammetry (CV) cures of (a) CTOCN-750, (b) CTG5-750, (c) CTG10-750, (d) CTG20-750, (e) CTOCN-1100 and (f) CTG10-1100 at different scan rates

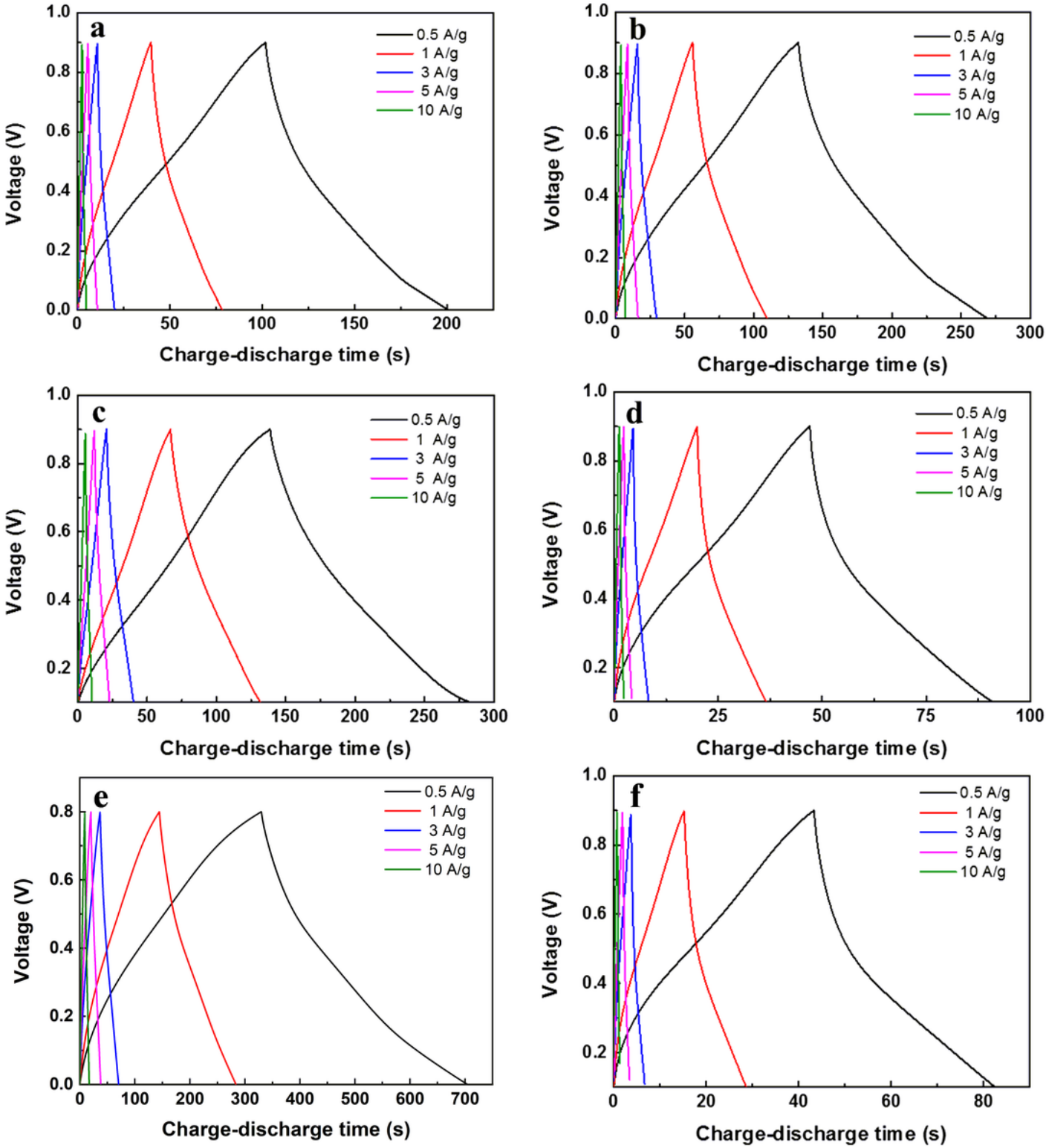

Figure 5

Galvanostatic charge-discharge curves of (a) CTOCN-750, (b) CTG5-750, (c) CTG10-750, (d) CTG20-750, (e) CTOCN-1100 and (f) CTG10-1100 at different current densities.

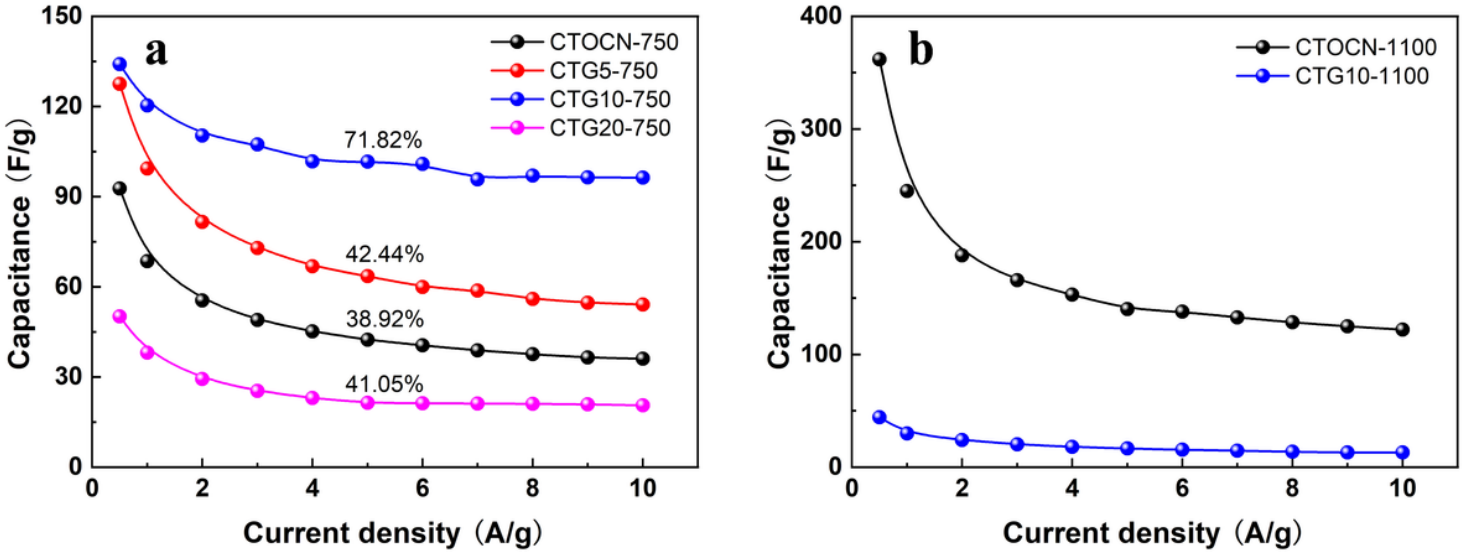

Figure 6

Specific capacity of (a) CTG-750 samples with different graphene loadings and (b) CTG-1100 samples as a function of current density ranging from 0.5 A/g to 10 A/g

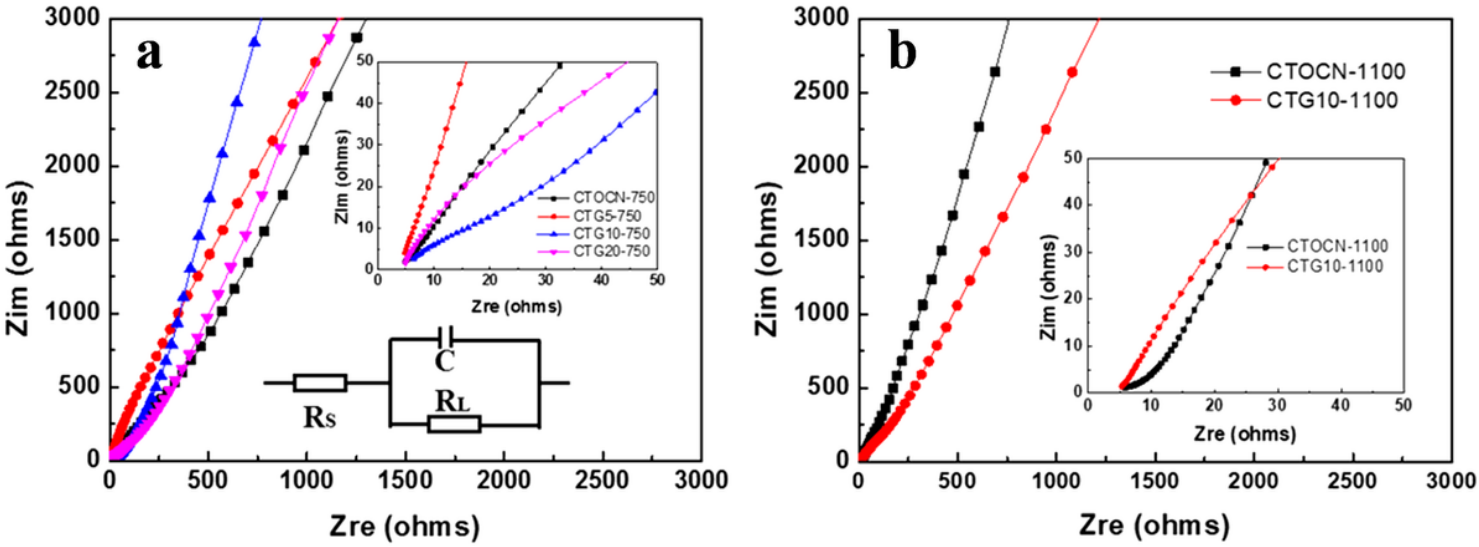

Figure 7

Nyquist impedance spectra of (a) CTG-750 samples with different PG loadings and (b) CTG-1100 samples

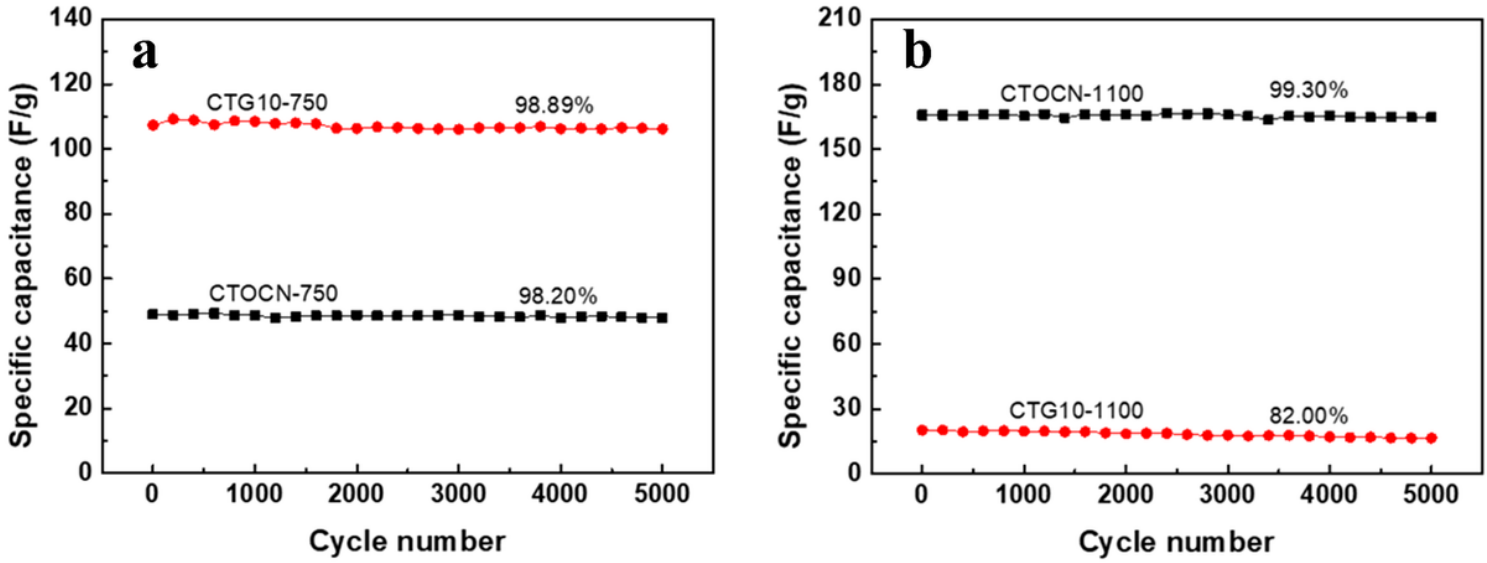

Figure 8

Cycling stability of (a) CTOCN-750, CTG10-750 and (b) CTOCN-1100, CTG10-1100 over 5000 cycles at a current density of 3 A/g

Supplementary Files

This is a list of supplementary files associated with this preprint. Click to download.

- SupportingInformation.docx
- Graphicalabstract.png